A Novel Decentralized Droop Control Scheme for Multiparalleled APFs With Grid Current Detected

Zhilong Zhang, *Student Member, IEEE*, Hao Yi, *Member, IEEE*, Yuguo Li, *Student Member, IEEE*, Xin Jiang, *Student Member, IEEE*, Zhenxiong Wang, *Member, IEEE*, and Fang Zhuo, *Member, IEEE*

***Abstract*—With the development of renewable energy generation, a single active power filter (APF) can hardly satisfy the requirements for harmonic compensation in high-power applications. Consequently, APFs are frequently connected in parallel to boost the capacity. And a central controller or a communication line is employed to allocate the compensation capacity. However, the intercommunication among APFs not only diminishes the reliability of the system, but also deteriorates the dynamic response. Additionally, hardware modifications must be applied to the original single APFs. Therefore, this article proposes a novel decentralized droop control scheme for multiparalleled APFs. With grid current detected, the proposed scheme enables the APFs to automatically allocate the compensation current. In comparison with prior research, both harmonic filtering and current sharing exhibit substantial enhancements, while dynamic response is maintained. Besides, the proposed scheme is more suitable for N multiparalleled APFs with lower steady error and better reliability. The detailed operating principle, parameter tuning, and performance analysis are presented. Finally, the proposed scheme is verified by simulations and experiments under various operating conditions.**

***Index Terms*—Decentralized control, grid current detected control, multiparalleled active power filter (APF), stability analysis.**

I. Introduction

With the rapid development of renewable generation in the last decade, the massive utilization of power electronics devices has significantly deteriorated the power quality. To guarantee power quality, active power filters (APFs) have been proposed to compensate for the harmonics [1], [2], [3]. However, in high-power applications, a single APF is required to have high-rated current [4]. In this case, the inverter cannot operate at a high switching frequency, thereby leaving harmonics not completely compensated [5], [6]. In contrast, the other popular solution comes to multiparalleled APFs with smaller rated capacity. Compared with single APF, multiparalleled APFs scheme is superior in boosting the total compensation capacity [7], [8]. Besides, the ability to operate at higher switching frequency, the multiparalleled APFs offer notable advantages in mass production and on-site maintenance [9]. Additionally, it is more convenient for multiparalleled APFs to implement redundancy control and capacity expansion. When an APF fails or is taken offline for maintenance, the multiparalleled APFs can automatically reallocate the compensation capacity.

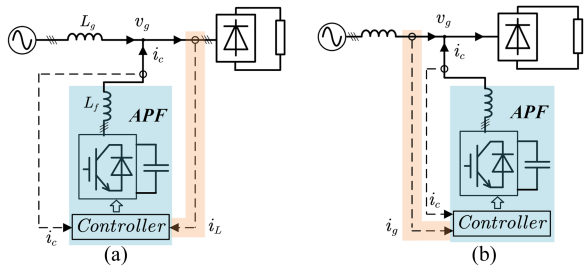

Fig. 1. Basic control schemes of single APF. (a) Load current detected control. (b) Grid current detected control.

The primary control schemes of single APF include load current detected control and grid current detected control [10]. The classification is based on the location of current detector as depicted in Fig. 1. As [11] illustrates, the load current detected control detects the nonlinear load's current as compensation current reference of APF, forming an open-loop control. The latter aims to regulate the grid current directly, forming a closed-loop control [12]. In [13], it has been pointed out that the load current detected control performs better dynamic response. And the grid current detected control owns better filtering performance. In practical applications, load current detected control is more popular due to its simpler implementation.

Consequently, based on load current detected control, various multiparalleled APFs schemes have been proposed with a central controller or communication line employed. First, a scheme called "power splitting mode" with a central controller is presented in [14] and [15]. In this scheme, the allocation capacity is assigned in proportion to the rated capacity and reallocation can be achieved by the central controller. However, the reliability of this scheme is restricted by the central controller. In industrial conditions, the failure in communication will destroy the capacity allocation and introduce more harmonics. Furthermore, the "distributed power splitting mode" is proposed in [16] as an enhancement that removes the central controller. However, redundancy control is also eliminated in this scheme due to the absence of the central controller. Additionally, an "frequency

Received 14 September 2024; revised 30 October 2024; accepted 30 November 2024. Date of publication 4 December 2024; date of current version 28 January 2025. This work was supported by the National Key R&D Program of China under Grant 2023YFB2407500. Recommended for publication by Associate Editor S. Golestan. *(Corresponding author: Hao Yi.)*

The authors are with the State Key Laboratory of Electrical Insulation and Power Equipment, Xi'an Jiaotong University, Xi'an 710049, China (e-mail: zl0502@stu.xjtu.edu.cn; yi_hao@xjtu.edu.cn; liyuguo0227@163.com; 3120104229@stu.xjtu.edu.cn; wzhenxiong@xjtu.edu.cn; zffz@xjtu.edu.cn).

Color versions of one or more figures in this article are available at https://doi.org/10.1109/TPEL.2024.3510754.

Digital Object Identifier 10.1109/TPEL.2024.3510754

splitting mode" scheme has been mentioned in [17]. In this scheme, the APFs with larger capacities are dedicated to the compensation of low-frequency harmonics, while those with smaller capacities are assigned to high-frequency harmonics. Nevertheless, the "frequency splitting mode" also requires a central controller, having the same limitations as the "power splitting mode." Besides, due to the absence of redundancy control, its filtering performance is highly influenced by the working conditions. Furthermore, a scheme is introduced based on grid current detected control, which manages to allocate the capacity proportionally [18], [19]. But it not only needs high switching frequency, but also results in circulating current among APFs. In [20] and [21], a dual-loop scheme that incorporates both grid/load current detected control has been proposed to utilize their advantages simultaneously. Due to the characteristics of open-loop control, the APFs with load current detected control in the multiparalleled system cannot sense the current of other APFs. Consequently, a central controller or a communication line is necessary to allocate the capacity in these schemes. And the incorporated central controller will not only diminish the reliability of the multiparalleled system, but also influence the dynamic response. Besides, additional hardware modifications need to be implemented on the original single APFs. It may be extremely difficult when the multiparalleled APFs are of different types.

Therefore, to achieve decentralized control without the central controller, previous research has tried to utilize different control strategies. A scheme called "current limitation mode" has been reported in [22]. In this scheme, the APFs are series arranged from load to the grid. Each APF compensates the harmonics the former APF left until reaching the capacity limitation. However, it fails to allocate the capacity properly and requires a significantly larger number of current sensors. For inverters operated as voltage sources in microgrids, the conventional droop-based control and its improvements are typically employed to achieve the harmonic current sharing [23], [24]. The droop-based control has realized the current sharing by modifying the effective line impedance of inverters [25], [26]. However, there exists a tradeoff between power quality and current sharing effectiveness. And similar solutions can not be directly applied in the case of multiparalleled APFs Conventional droop-based control is established on the voltage relationship. But APF is operated as a current source. In addition, conventional droop-based control is designed to share harmonics among all inverters in the microgrid. And it will lose its effect when being connected to the grid. The multiparalleled APFs, in contrast, aim to compensate for harmonics and share them exclusively among APFs. Consequently, efforts have been made to improve traditional droop-based control for APFs [27]. In [28] and [29], the droop characteristics have been further modified with grid current detected control as Fig. 2. APFs are connected in parallel and detect the same grid current. In this way, the redundancy control and capacity allocation can be realized without communication. However, the filtering performance and allocation range of this scheme are restricted by the specific implementation structure. And the steady error will increase in proportion to the number of multiparalleled APFs. Besides, the

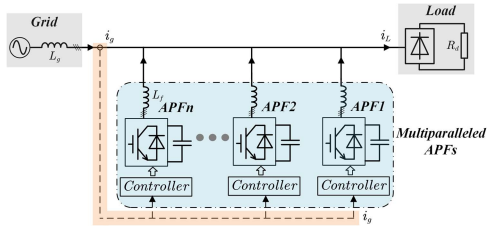

Fig. 2. Decentralized droop control scheme with grid current detected.

study on the droop coefficients tuning in this scheme still stays in the qualitative stage.

In this article, a novel decentralized droop control scheme is proposed for multiparalleled APFs with grid current detected. To establish the current droop relationship, conventional control structure of each APF is incorporated with additional droop control link and virtual resistor link in this scheme. By employing decentralized droop control, the APFs in the multiparalleled system can achieve redundancy control and capacity allocation automatically without communication. And robust performance is obtained when facing dynamic conditions. Furthermore, the proposed scheme demonstrates superior filtering performance and allocation range in comparison to the existing scheme. It is more suitable for the large number of paralleled APFs with lower steady error and better reliability. The detailed operating mechanism, performance analysis, and parameter tuning are presented in this article.

The rest of this article is organized as follows. Section II explains the basic control method of APF and points out the main issues that emerged in multiparalleled APFs. Section III illustrates the implementation and mechanism of the proposed scheme. Besides, performance analysis and parameter tuning are also presented. Section IV discusses the performance comparison between the proposed scheme and the existing scheme. The results of simulations and experiments are shown in Section V. Finally, Section VI concludes this article.

II. Basic Control Methods and Main Issues Emerged in Multiparalleled APFs

As demonstrated by previous studies [29], the basis of the current droop allocation of APFs is closed-loop control. Consequently, the grid current detected control is frequently utilized to achieve the current sharing. The grid current detected control methods mainly include: 1) current source based (CS) method and 2) power balance based (PB) method. And their control diagrams are depicted in Fig. 3. As Fig. 3(a) shows, the CS method forms a cascaded double-loop control structure that includes harmonic compensation loop and inner current loop. In this manner, harmonic compensation's dynamic response can be conveniently modified. Nevertheless, the cascaded structure will inevitably result in the coupling of two loops. And the coupling will generate the conflict between system stability and filtering performance. With the CS method employed, the allocation precision of the existing decentralized scheme is also in conflict with its filtering performance.

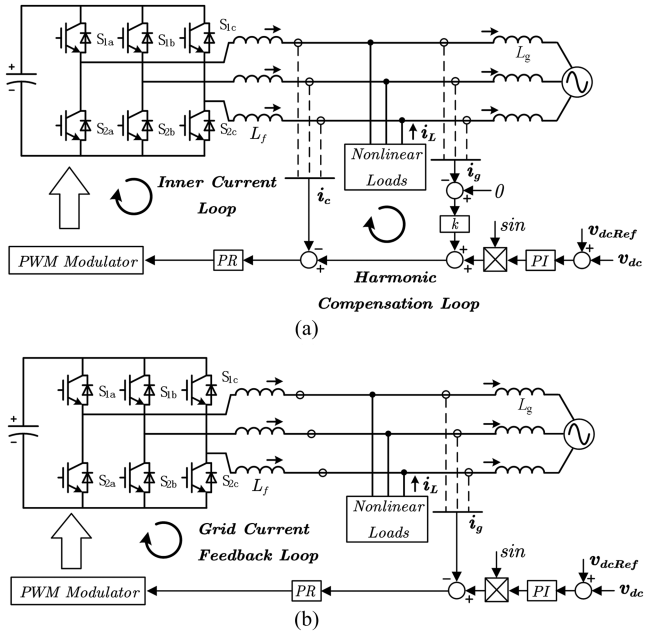

Fig. 3. Control diagrams of methods with grid current detected control. (a) CS method. (b) PB method.

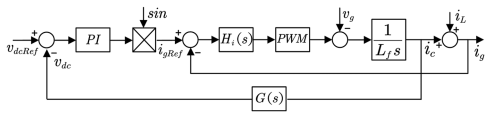

Fig. 4. Detailed control block diagram of PB method in single APF.

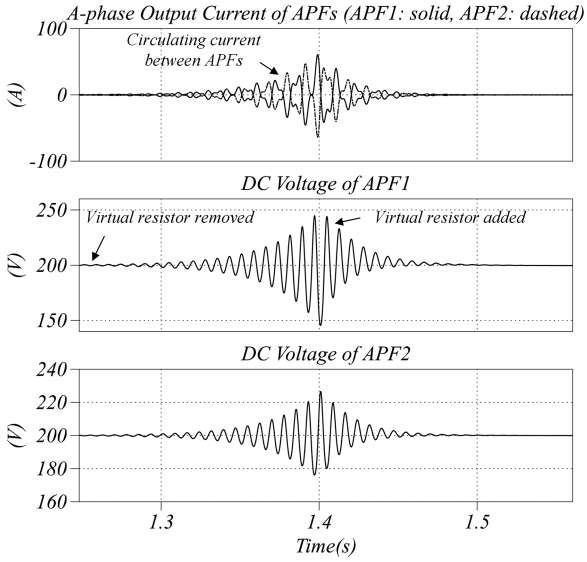

Fig. 5. Circulating current phenomenon in multiparalleled APFs with PB method.

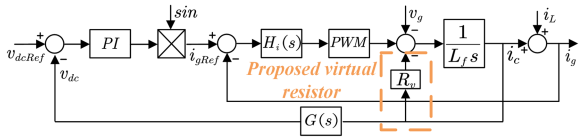

Fig. 6. Modified PB control block diagram with the proposed virtual resistor.

Consequently, the PB method is employed in this article to address the drawbacks of the CS method. As Fig. 3(b) depicts, the PB method adopts an interactive double-loop structure to achieve both harmonic compensation and dc voltage control. Its detailed control diagram is depicted in Fig. 4. In this way, the two loops share the performance of one controller $H_i(s)$, thereby avoiding the conflict in CS method. The controller $H_i(s)$ is configured as multi-PR controller for 5th, 7th, 11th, and 13th harmonics as follows [30]:

$$PR(s) = H_i \ \ (s) = k_p + \sum_k \frac{K_{rk}}{s - jk\omega_1}. \tag{1}$$

In (1), K_{rk} is the coefficient of the PR controller and ω_1 represents the fundamental frequency. In Fig. 4, $G(s)$ represents the impact of APF current i_c on dc voltage v_{dc}, whose expression is introduced in [31]. And the transfer function of harmonic compensation in the PB method can be calculated as follows:

$$\frac{i_g}{i_L} = \frac{L_f s}{L_f s + H_i(s) G_d(s)} \tag{2}$$

$$G_d(s) = e^{-1.5 T_d s}. \tag{3}$$

In (2), L_f is the filter inductor of APF and $G_d(s)$ represents the control delay of the system as (3). In (3), T_d is the sampling time [32]. As (2) reveals, the PB method could compensate the harmonics completely, as the harmonics in grid current will be diminished to 0 by the resonant controllers in $H_i(s)$.

The analysis and verification of the PB method in a single APF have been conducted in previous research. However, in the practical application of multiparalleled APFs, the PB method will encounter two main issues including: 1) circulating power flow and 2) random harmonic sharing. As harmonic sharing is the main topic discussed in this article, the basic cause, waveform, and available stabilization method of circulating power flow will be briefly introduced as follows. And detailed analysis will be carried out in future research.

In multiparalleled APFs, each APF detects the same grid current i_g as the control target. Therefore, as the multicontrolled object, grid current responds relatively slower in multiparalleled APFs [13]. Once the multiparalleled APFs are activated, the active power is required to charge the dc capacitors of APFs. However, as the grid current i_g is unable to respond rapidly, active power is circulating among APFs as Fig. 5. According to Fig. 5, it is shown that the oscillation of dc voltage is gradually increasing and the waveforms of each APF are symmetry. Besides, the overall output active power remains zero, indicating the circulating power flow.

The critical reason for this issue lies in the undamped active power circulating path among the multiparalleled APFs. Therefore, an additional virtual resistor is proposed to damp the power circulating path. The modified control diagram of the PB method is shown in Fig. 6. With the proposed damping method, the output filter L_f is equivalently series connected with a virtual

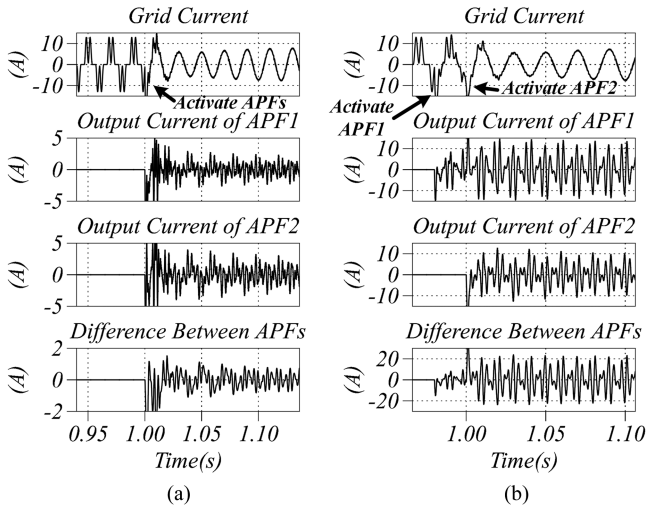

Fig. 7. Current allocation of multiparalleled APFs in different cases. (a) APFs are activated simultaneously. (b) APF1 is activated first.

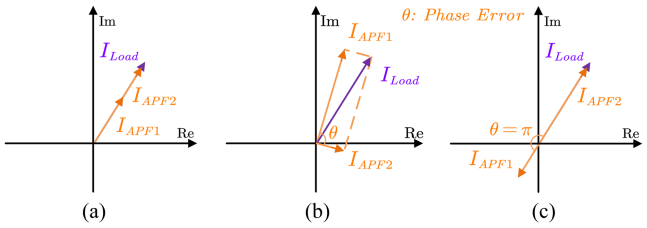

Fig. 8. Different current allocation situations without control. (a) No phase error exists. (b) Phase error exists. (c) Worst case: phase error $= \pi$.

resistor R_v. And the power oscillation of APFs can be damped as Fig. 5 depicts.

By employing the proposed virtual resistor, the multiparalleled APFs can be operated in parallel without the emergence of circulating power flow. However, in practical applications, the current sharing of APFs is typically random. In Fig. 7, two multiparalleled APFs are activated at approximately $t = 1.0s$ to compensate for the harmonics. However, in comparison with Fig. 7(a) and (b), different activation orders result in varying current sharing states. In Fig. 7(a), equal current sharing can not be guaranteed even if APFs are activated simultaneously. Besides, the phase error can be observed in Fig. 7(b), resulting in the unnecessary compensation current. This uncontrolled current sharing not only wastes the redundancy capacity. It will also decrease the compensation efficiency as phase error exists. Fig. 8 depicts different operating cases where phase error exists among compensation current. In these cases, multiparalleled APFs still manage to achieve the harmonic compensation ($I_{APF1} + I_{APF2} = I_{Load}$). However, in the cases as Fig. 8(b) and (c), the consumed compensation capacity ($|I_{APF1}| + |I_{APF2}|$) is much larger than the needed capacity (I_{Load}), which results in the unbearable decreased efficiency. Therefore, it is vital to realize suitable current sharing.

This section presents the PB control method of a single APF and illustrates the main issues that emerged in multiparalleled

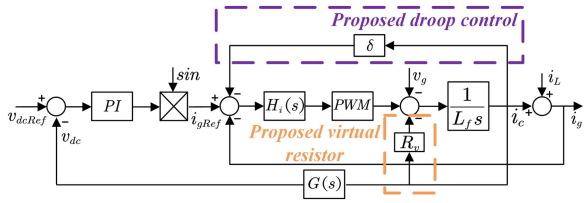

Fig. 9. Control block diagram of single APF with proposed droop control and virtual resistor.

APFs including 1) circulating power flow and 2) current sharing. As the former is not the main topic of this article, a simple virtual resistor is proposed to avoid the circulating power. In this way, the APFs can be connected in parallel as Fig. 2.

III. Proposed Decentralized Droop Control Scheme

A. Proposed Decentralized Droop Control

As illustrated in Section II, the uncontrolled current sharing will lead to an unbearable efficiency decrease. Therefore, this article proposes a decentralized droop control method to achieve automatic current sharing. The detailed control block diagram with the proposed scheme is depicted in Fig. 9. In the decentralized droop scheme, an additional feedback path is incorporated. The load current i_c is fed back into the current control loop with droop coefficient δ. According to Fig. 9, the transfer function from i_L to i_g can be obtained as (4).

$$\frac{i_g}{i_L} = G_c(s) = \frac{L_f s + R_v + \delta H_i(s) G_d(s)}{L_f s + R_v + (1+\delta) H_i(s) G_d(s)} \tag{4}$$

$$e_{ss} = \lim_{s \to jk\omega_1} G_c(s) = \frac{1}{1 + \frac{1}{\delta}}. \tag{5}$$

Compared to the conventional scheme in (2), the proposed scheme modifies the filtering performance mainly by droop coefficient δ in (4). Its filtering steady error is expressed as e_{ss}. As the proposed scheme is designed for harmonics with specific orders, the resonant controller $H_i(s)$ will exhibit infinite gain at these frequency points. Therefore, the e_{ss} could be simplified as (5) for the specific harmonics. According to (5), the steady error is positively correlated with δ. Consequently, in order to decrease the steady error and maintain the filtering performance, the value of δ should be set below 0.05.

To clarify the mechanism of proposed decentralized control more clearly, an example of two APF modules is depicted in Fig. 10 which omits the dc control link. In the multiparalleled APFs as Fig. 10(a), each APF detects the grid current back into its current controller. In this way, the output current of the other APF can be sensed without communication. Except for the proposed droop control link, the transfer function of current control can be calculated as $G_o(s)$ in the following equation:

$$G_o(s) = \frac{H_i(s) G_d(s)}{L_f s + R_v}. \tag{6}$$

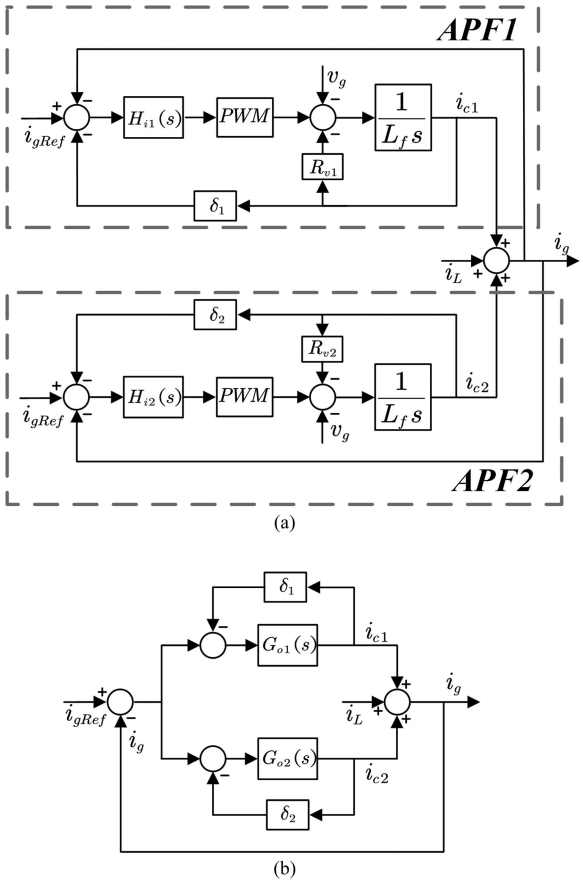

Fig. 10. Overall control block diagram of the system comprising of two APFs. (a) Detailed diagram. (b) Simplified diagram.

With simplified current control link, Fig. 10(a) can be equivalently transformed into Fig. 10(b). And Fig. 10(b) shows the harmonic compensation and current sharing process more clearly. Two APFs operate to control the grid current collectively and each APF serves as a separate controller.

In Fig. 10(b), the droop control establishes the relationship between grid current i_g and output current i_{c1}, i_{c2} with droop coefficients. In this way, each APF could sense the output current of other APFs by i_g. Their specific signal transmission relationship can be expressed in (7) as Fig. 10(b) shows.

$$\begin{cases} i_g = i_L + i_{c1} + i_{c2} \\ i_{c1} = G_{o1}\ (s)\ (-i_g - \delta_1 i_{c1}) = \frac{H_{i1}(s)G_d(s)}{L_f s + R_{v1}}\ (-i_g - \delta_1 i_{c1}) \\ i_{c2} = G_{o2}\ (s)\,(-i_g - \delta_2 i_{c2}) = \frac{H_{i2}(s)G_d(s)}{L_f s + R_{v2}}\,(-i_g - \delta_2 i_{c2}) \end{cases}. \tag{7}$$

As grid current i_g associates the multiparalleled APFs, the latter two equations in (7) can be calculated as (8). In (8), the transfer function from i_g to i_c is expressed.

$$\begin{cases} i_{c1} = -\frac{H_{i1}(s)G_d(s)}{L_f s + R_{v1} + \delta_1 H_{i1}(s)G_d(s)} i_g \\ i_{c2} = -\frac{H_{i2}(s)G_d(s)}{L_f s + R_{v2} + \delta_2 H_{i2}(s)G_d(s)} i_g \end{cases}. \tag{8}$$

According to (8), the current sharing relationship between i_{c1} and i_{c2} can be obtained as (9) by substituting i_g in (8). Furthermore, (9) can be simplified to (10) as the resonant controller in $H_i(s)$ exhibits infinite gain for the specific harmonics (5th, 7th, 11th, 13th…).

$$\frac{i_{c1}}{i_{c2}} = \frac{\frac{L_f s + R_{v2}}{H_{i2}(s)G_d(s)} + \delta_2}{\frac{L_f s + R_{v1}}{H_{i1}(s)G_d(s)} + \delta_1} \tag{9}$$

$$\lim_{s \to jk\omega_1} \frac{i_{c1}}{i_{c2}} = \lim_{s \to jk\omega_1} \frac{\frac{L_f s + R_{v2}}{H_{i2}(s)G_d(s)} + \delta_2}{\frac{L_f s + R_{v1}}{H_{i1}(s)G_d(s)} + \delta_1} = \frac{\delta_2}{\delta_1}. \tag{10}$$

It can be inferred from (10) that the proposed decentralized droop control could achieve the current sharing for the designed specific harmonics. And the allocation ratio is solely determined by the preset droop coefficients δ_1, δ_2 for various types of APFs, demonstrating excellent feasibility. Besides, as both δ_1 and δ_2 are constant parameters, there will be no phase error among APFs, thereby avoiding the decreased compensation efficiency. Similarly, the droop characteristics in n multiparalleled APFs could be established as (11) with the proposed scheme. In (11), n represents the number of APFs.

$$\delta_1\ i_{c1} = \delta_2\ \ i_{c2} = \cdots = \delta_n\ i_{cn}. \tag{11}$$

As (11) indicates, the current droop relationship is formed in each APF. The current allocation could be modified by the droop coefficients. For specific APF, the smaller δ_n is assigned, the larger output current is allocated. Therefore, by appropriately setting the values of droop coefficients, the APFs can be modified to share the harmonic compensation current in the ratio of their current ratings. When a specific APF fails or is taken offline, it could be directly disconnected from the system. The proposed scheme will automatically relocate the current among other APFs in this case.

In this section, the control scheme and underlying current sharing mechanism of the proposed scheme have been presented. With the maintained filtering performance, the proposed decentralized method manages to achieve automatic capacity droop allocation of multiparalleled APFs without communication or capacity waste.

B. Steady/Dynamic Performance and Stability Analysis of Multiparalleled APFs Considering Parameter Variations

The current allocation of the proposed scheme has been verified. Furthermore, the dynamic/steady performance of multiparalleled APFs should be evaluated. The steady error, system stability, and dynamic response of current sharing are analyzed in this section, considering the variations of critical parameters (filter inductor, number of APFs, and controllers' gain).

First, to analyze the steady error of harmonic compensation, transfer function $G_{PB}(s)$ from i_g to i_L could be obtained as (12) according to Fig. 10(b). For designed specific harmonics, it can be simplified to (13) and represent the steady error e_{ss_PB}.

$$\frac{i_g}{i_L} = G_{PB}\ \ (s) = \frac{1}{1 + \frac{G_{o1}(s)}{1+\delta_1 G_{o1}(s)} + \frac{G_{o2}(s)}{1+\delta_2 G_{o2}(s)}} \tag{12}$$

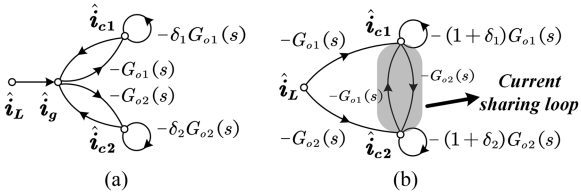

Fig. 11. Signal flow diagram of multiparalleled APFs with the proposed droop control. (a) Original signal flow diagram. (b) Interactive relationship between compensation current.

$$e_{ss\_PB} = \lim_{s \to jk\omega_1} G_{PB}(s) = \frac{1}{1 + \frac{1}{\delta_1} + \frac{1}{\delta_2}}. \tag{13}$$

Similarly, for a generic case involving "n" APFs, the steady-state error can be expressed as follows:

$$e_{ss\_PB} = \frac{1}{1 + \sum_{i=1}^{n} \frac{1}{\delta_i}}. \tag{14}$$

According to (14), the steady error is only relevant with the preset droop coefficients and number of APFs. The other critical parameters (filter inductors, controllers' gain, inverters' structure…) will not significantly influence the steady error when the proposed scheme is applied. Compared with the case of a single APF in (5), the steady error of multiparalleled APFs becomes smaller with more APFs installed. It reveals that the steady error of the whole APF system will be smaller than that of any specific APF operating alone. Therefore, even if several APFs fail or are taken for maintenance, the other APFs will be reallocated automatically. And the filtering performance will not be greatly deteriorated.

Furthermore, to investigate the stability of current sharing, Fig. 10 is simplified to the signal flow diagram Fig. 11(a). If harmonics are generated in load current $\hat{i}_L$, they will be detected in the grid current $\hat{i}_g$. And compensation current $\hat{i}_{c1}$ and $\hat{i}_{c2}$ is generated by current control and then injected into grid current. Besides, the proposed droop control adds additional self-feedback loops of compensation current. With the proposed scheme introduced, the output current $\hat{i}_{c1}$ and $\hat{i}_{c2}$ are associated with each other. Therefore, Fig. 11(b) is depicted to demonstrate the underlying current sharing loop between $\hat{i}_{c1}$ and $\hat{i}_{c2}$ by cancelling out the grid current in Fig. 10(a). The loop gain $L(s)$ between i_{c1} and i_{c2} could be obtained as follows:

$$L(s) = -\frac{G_{o1}(s)}{1 + (1+\delta_1) G_{o1}(s)} \frac{G_{o2}(s)}{1 + (1+\delta_2) G_{o2}(s)}. \tag{15}$$

The Nyquist diagram of $L(s)$ is depicted in Fig. 12 with different droop coefficients. As Fig. 12 shows, when the coefficients are assigned negative, the positive feedback current sharing loop will be formed as the curve circles around $(-1, 0)$. It will seriously deteriorate the stability of the system. In comparison, when the coefficients are assigned positive, the curve will not cross $(-1, 0)$ equivalently, thereby maintaining stability. Thus, the values of droop coefficients are recommended to be assigned greater than zero. Furthermore, Figs. 13 and 14 depict the Nyquist diagrams of $L(s)$ with different parameters.

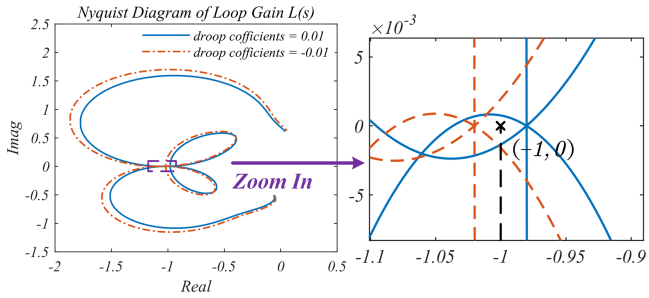

Fig. 12. Nyquist diagram of current sharing loop gain $L(s)$ considering -500 to 500 Hz.

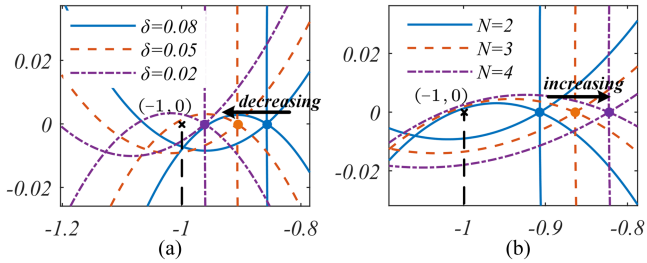

Fig. 13. Nyquist diagram of $L(s)$ considering parameter variations in droop control. (a) Droop coefficients. (b) Number of multiparalleled APFs.

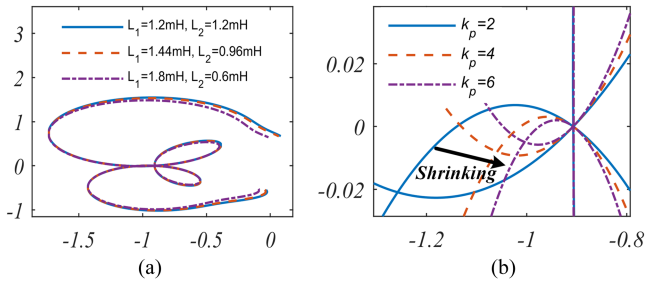

Fig. 14. Nyquist diagram of $L(s)$ considering parameter variations in current control. (a) Filter inductors. (b) Proportional gain k_p.

In Fig. 13, the influence of parameter variations in droop control is assessed. As the droop coefficients in Fig. 13(a) decrease, the crossing point is approaching $(-1,0)$, indicating the reduced stability margin. However, the system stability is not substantially impacted by the change, as it is modest. In Fig. 13(b), the stability is investigated in relation to the number of multiparalleled APFs. It shows that the stability margin is increasing with more installed APFs. And the impact of filter inductors and controllers' gain is shown in Fig. 14. As Fig. 14(a) and (b) demonstrate, the parameter variations of current control link have little influence on the stability of current sharing. According to the abovementioned analysis, the stability of current sharing is mainly determined by the proposed droop control. Larger droop coefficients and a greater number of APFs lead to better system stability.

Furthermore, the pole-zero diagram of the closed-loop transfer function $G_{PB}(s)$ is depicted in Fig. 15 to analyze the dynamic response. According to the control theory, the system

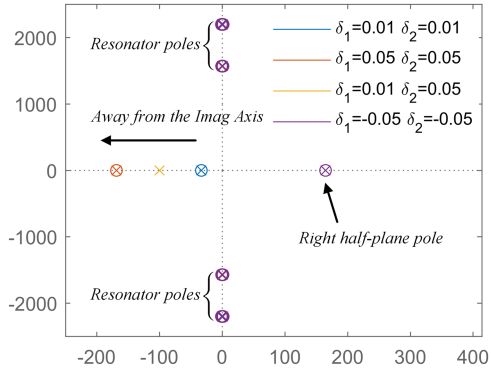

Fig. 15. Pole-zero map of closed-loop function $G_{PB}(s)$ with different droop coefficients assigned considering -500 to 500 Hz.

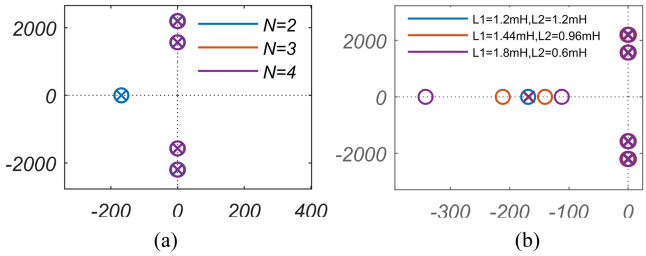

Fig. 16. Pole-zero map of closed-loop function $G_{PB}(s)$ considering parameter variations. (a) Number of multiparalleled APFs. (b) Filter inductors.

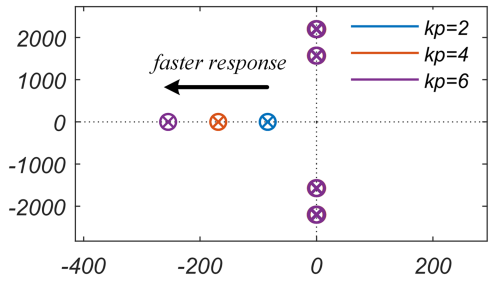

Fig. 17. Pole-zero map of closed-loop function $G_{PB}(s)$ considering variations of controllers' gain k_p.

poles reflect the dynamic response of the system. In Fig. 15, the poles around the imaginary axis are introduced by the resonant controllers at fifth and seventh harmonic. Besides, with the increasing droop coefficients, the dominant pole gradually moves away from the imaginary axis, indicating faster response and less oscillation in the current sharing process. In multiparalleled systems, the dominant pole is affected by all APFs as Fig. 15 shows. In this case, the dominant pole is located in the average position of all APFs' zeros. Additionally, if the coefficients are assigned negative, the dominant pole will be in the right half-plane as the purple point, destroying the stability. Figs. 16 and 17 illustrate the change trend of poles with parameter variations. In Fig. 16(a) and (b), the parameter variations of APFs' number and filter inductors are considered. However, the results show that these parameter variations will not influence the poles evidently. And the impact of controllers' gain on the dynamic response is assessed in Fig. 17. With the increasing proportional gain k_p,

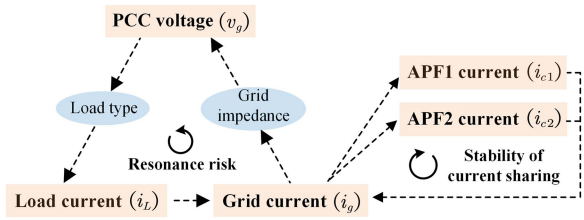

Fig. 18. Underlying mechanism of resonance risk when multiparalleled APFs are operated.

the poles are moving away from the imaginary axis, indicating a faster response.

In this section, the steady error, system stability, and dynamic response of the proposed scheme are analyzed considering parameter variations.

1) The steady error of harmonic filtering is only associated with droop coefficients and number of APFs. The larger coefficients are, the higher steady error is. And the steady error of multiparalleled APFs is smaller than that of any APF operating alone. Therefore, the steady error of the proposed decentralized scheme is guaranteed.
2) The stability of current sharing also depends on the droop coefficients and APFs' number. The impact of other parameter variations is modest. With positive droop coefficients assigned, system stability is ensured. Larger droop coefficients and a greater number of APFs will lead to a larger stability margin.
3) The dynamic response is mainly in relation to droop coefficients and controllers' gain. Dynamic response speed can be improved by enlarging droop coefficients and controllers' gain. Besides, variations of filter inductors and APFs' number have little influence on the dynamic response of current sharing.

For the proposed scheme, the stability and steady error will be improved with more APFs installed. Consequently, there are no scalability limitations in terms of current sharing. However, the scalability limitation truly exists in practical applications regardless of the scheme employed. The multiparalleled APFs will suffer from the resonance risk with the increasing parallel number [9]. Fig. 18 provides the illustration of potential resonance risk. When multiparalleled APFs compensate for the harmonics, the interactive relationship is formed among PCC voltage, load current, and grid current [10]. And the resonance might be induced by the feedback loop in Fig. 18. In this process, the dynamic response of APFs' control scheme is also involved. Although the inner stability of current sharing is maintained, increasing number of APFs still might excite the outer resonance. On one hand, increasing number of APFs will improve the filtering performance, which is more likely to result in resonance. On the other hand, more installed APFs will negatively damp the system [11]. Fig. 19 depicts the simulation waveforms when the resonance is triggered. And amplitude of APF1's 13th harmonic current is shown to reflect the dynamic. In Fig. 19(a), system remains stable when APF1 is operating alone. However, resonance occurs when APF2 is also employed to share the harmonics in Fig. 19(b). The resonance can be

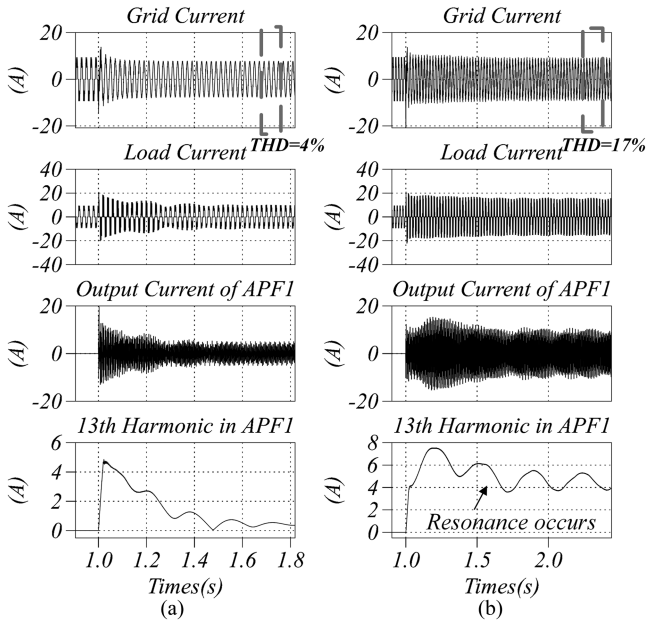

Fig. 19. Waveforms to verify the scalability limitation of resonance risk. (a) APF1 is operating alone. (b) APF1 and APF2 are operated in parallel.

observed in both load current and APF1's current. Harmonics are amplified and THD increases from 4% to 17%. It verifies the existence of scalability limitations regarding resonance risk. Besides, the resonance characteristics are also highly associated with load type and grid impedance [3]. Larger grid impedance and voltage-source load will substantially increase the risk. Consequently, the scalability limitation of resonance risk is hard to be specified, which is another broader research topic. And we have listed it as a possible future work.

C. Algorithm for Parameter Tuning of Droop Coefficients

According to the droop characteristics in (11), there are many sets of parameters to meet the demands of current sharing. And the choice of droop coefficients is a tradeoff between filtering performance and response speed. Thus, this article proposes an algorithm to determine the balanced droop coefficients.

Step 1: Identify the APF which has the minimum rated current (I_{min}) among multiparalleled APFs.

Step 2: Determine the upper limit of steady error (δ_{max}) in multiparalleled APFs. According to the abovementioned analysis, the value is also the steady error when the APF with minimum rated current is operating alone. It is typically set below 0.05.

Step 3: Set the upper limit of steady error as the droop coefficient of APF which has the minimum rated current.

Step 4: Calculate droop coefficients (δ_j) of each APF in the multiparalleled system according to their rated current (I_j) as follows:

$$\delta_j = \frac{I_{min}\delta_{max}}{I_j}. \tag{16}$$

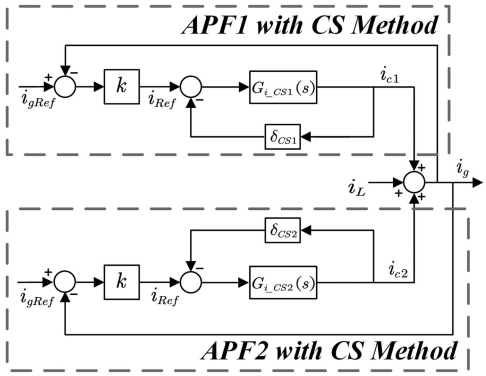

Fig. 20. Overall control block diagram of the system comprising of two APFs with CS method.

In this way, the proposed algorithm could achieve the current sharing in proportion to the capacity of each APF.

IV. Comparison Between Proposed Decentralized Droop Scheme and Existing Scheme

As illustrated in Section III, the existing scheme is mainly based on the structure of the CS method [26], which is different from the proposed scheme. And it is found that their main difference lies in filtering performance, allocation range, and system stability. The double-loop structure of the CS method will lead to the mutual restriction between filtering performance and allocation range in multiparalleled APFs. And the system stability of the CS method will be diminished with higher filtering demand. In these aspects, the proposed scheme behaves better than the existing one. But its response speed is relatively slower, which is acceptable. Because the droop allocation is a slow process itself.

A. Comparison in Filtering Performance and Allocation Range

The control block diagram of the existing method is depicted in Fig. 20, comprising two multiparalleled APFs. In Fig. 20, δ_{CS1}, δ_{CS2} are the preset droop coefficients. And the closed-loop function $G_{i\_CS}(s)$ of current loop can be calculated as follows:

$$G_{i\_CS}\ (s) = \frac{H_i\,(s)\,G_d\,(s)}{L_f s + H_i\,(s)\,G_d\,(s)}\,. \tag{17}$$

Similar to the proposed scheme, the transfer function $G_{CS}(s)$ from i_g to i_L can be obtained as (18). And (18) can be simplified to (19) for specific harmonics to calculate the steady error e_{cs}.

$$G_{CS}\,(s) = \frac{1}{1 + \frac{kG_{i_{CS1}}(s)}{1+\delta_{CS1}G_{i_{CS1}}(s)} + \frac{kG_{i_{CS2}}(s)}{1+\delta_{CS2}G_{i_{CS2}}(s)}} \tag{18}$$

$$e_{cs} = \lim_{s\to jk\omega_1} G_{CS}\,(s) = \frac{1}{1 + \frac{k}{1+\delta_{CS1}} + \frac{k}{1+\delta_{CS2}}}. \tag{19}$$

Furthermore, the droop relationship of the existing scheme can be obtained in (20) in the same manner as the proposed

scheme.

$$(1+\delta_{CS1})\ i_{c1} = (1+\delta_{CS2})\ \ i_{c2} = \cdots = (1+\delta_{CSn})\ i_{cn}. \tag{20}$$

Based on the parameter assigning method in [28] and [29], the droop coefficient of APF which has the maximum rated current is assigned to be 1. And the other APFs' droop coefficients are assigned values larger than 1. However, the steady error will be increased in this existing method with different allocations. The steady error e_{cs} of n multiparalleled APFs has been shown in (19). In (19), $k/(1+\delta_{CSn})$ represents the steady error part contributed by corresponding APF. Once the capacity allocation is changed, the droop coefficient of specific APF will be increased. And the corresponding steady error will also increase, as $k/(1+\delta_{CSn})$ is in the denominator of e_{cs}. Besides, the large preset droop coefficient will seriously deteriorate the filtering performance when APF is operating alone. The case of two parallel APFs is taken as an example. When the allocation changes from 1:1 to 1: m, the steady error e_{cs1} is increased to e_{cs2} as (21). And the steady error is positively correlated with parameter m.

$$\begin{cases} e_{cs1} = \frac{1}{1+k} \\ e_{cs2} = \frac{1}{1+\frac{k}{2}+\frac{k}{2m}} \end{cases}. \tag{21}$$

In comparison, the steady error e_{ss} of the proposed scheme is shown in (14). When the allocation changes, the upper limit of steady error is guaranteed. And the droop coefficient is assigned smaller with larger allocated capacity. It can be found that this allocation characteristic is opposite from that of the existing method. Therefore, the steady error will be decreased with the proposed scheme in the same allocation. When the allocation changes from 1:1 to 1: m, the steady error e_{ss1} will be decreased to e_{ss2} as (22) assuming $\delta_1 = 2/k$.

$$\begin{cases} e_{ss1} = \frac{1}{1+k} \\ e_{ss2} = \frac{1}{1+\frac{m+1}{2}k} \end{cases}. \tag{22}$$

As the unbalanced allocation will increase the steady error, the allocation range of the existing scheme is restricted. When the upper limit of steady error is set as e_{cs_max}, the largest droop coefficients δ_{CSn} is restricted as follows:

$$\delta_{CSn} < \frac{k e_{cs\_max}}{1-e_{cs\_max}} - 1. \tag{23}$$

Therefore, with the restricted droop coefficient, the allocation range of the existing method is tightly restricted by the filtering performance. In comparison, as the capacity allocation will not increase the steady error, the proposed scheme has removed this constraint.

B. Comparison in System Stability and Dynamic Response

According to the analysis in Section III, the poles of the closed-loop transfer function determine the system stability and dynamic response. And closed-loop transfer function $G_{CS}(s)$ has been obtained as (18).

When the steady error remains consistent ($1/\ \delta_j = k/(1+\delta_{CSj})$), the pole-zero diagram of two control schemes is depicted in Fig. 21. In Fig. 21, blue/yellow points represent the proposed scheme and red/purple points represent the existing scheme under parameter variations. Compared with that of the proposed scheme, the existing scheme's dominant poles are relatively farther away from the imaginary axis. Nonetheless, considering their distance to the imaginary axis, the difference among poles is negligible. This demonstrates the similar dynamic response of the two schemes. Additionally, there are two conjugated poles in Fig. 21, which represent the high-frequency response. In Fig. 21, the close conjugated poles indicate the similar high-frequency performance of different schemes.

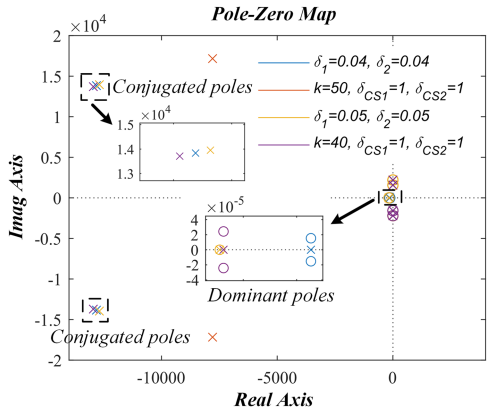

Fig. 21. Pole-zero map of proposed droop scheme and existing droop scheme.

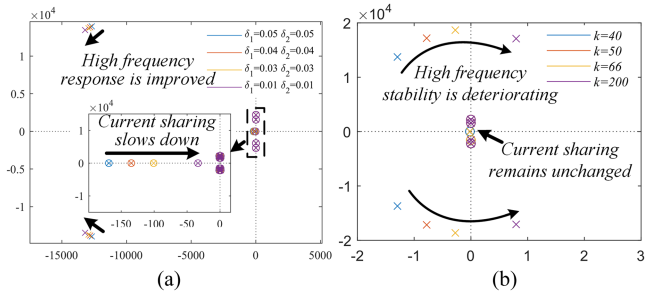

Fig. 22. Pole-zero maps of proposed scheme and existing scheme with better filtering performance. (a) Proposed scheme with increasing δ. (b) Existing scheme with increasing k.

However, when the filtering performance is enhanced in both schemes, the conjugated poles exhibit different variation trends as Fig. 22(a) and (b). For the proposed scheme, filtering performance is improved by decreasing droop coefficients δ. In Fig. 22(a), the poles move farther away from the imaginary axis when the droop coefficients are decreasing. And the dominant poles move closer to the zero point. It indicates that the stability of the proposed scheme is maintained and dynamic response pays the price. However, in the existing scheme as Fig. 22(b), filtering performance is modified by the control parameter k. In this case, the conjugated poles keep approaching the imaginary axis when k is increasing. And the poles will eventually move to the right half-plane, seriously deteriorating the high-frequency stability. In this process, the dominant poles remain unchanged,

TABLE I
COMPARISONS BETWEEN PROPOSED SCHEME AND EXISTING SCHEME

Schemes	Proposed scheme	Existing scheme
Filtering performance	Guaranteed	Deteriorated with unbalanced allocation
Allocation range	Broader	Limited
Dynamic response	Relatively slow	Fast
System stability	Better	Deteriorated with higher filtering demand

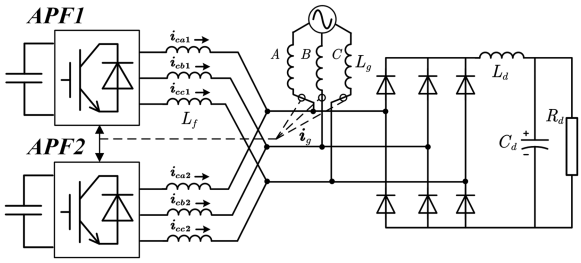

Fig. 23. Basic topology structure of simulation and experiment platform.

indicating the constant dynamic response. Therefore, the parameter k of existing scheme is typically restricted to maintain stability. Furthermore, the filtering performance is also limited by this restricted parameter.

In summary, specific comparisons between the proposed scheme and the existing scheme can be concluded in Table I. It can be found that the proposed scheme is more suitable for practical applications. Compared with existing schemes, it exhibits better filtering performance, allocation range, and system stability. The main drawback is the relatively slow dynamic response. However, droop allocation is a slow process itself and the proposed scheme could meet the requirements. Therefore, the proposed scheme is preferred to be adopted.

V. SIMULATIONS AND EXPERIMENTS

A. Simulations Under Various Operating Conditions

Detailed simulations are carried out in this section to verify the proposed scheme. The basic topology of the simulation is shown in Fig. 23. The load is selected as the three-phase uncontrolled rectifier. And two APFs are connected in parallel with grid current detected. In the simulations and experiments, the APFs are configured to compensate for the dominant harmonic (5th, 7th, 11th, 13th). The specific simulation parameters are listed in Table II.

In order to ascertain the analysis conclusions, several representative cases are chosen as follows: 1) two APFs compensate the harmonics in the ratio of 1:1; 2) two APFs compensate the harmonics in the ratio of 2:1; 3) three APFs compensate the harmonics in the ratio of 2:1:1; 4) one of the APFs ceases to operate during runtime; 5) multiparalleled APFs react to the sudden perturbation in the load current; 6) multiparalleled APFs with CS scheme react to the increasing filtering demand; 7) multiparalleled APFs with different control schemes react to the changed allocation.

TABLE II
SIMULATION PARAMETERS

Symbol	Parameter	Value
v_g	Grid voltage	60 V(RMS-phase)
v_{dc}	DC voltage of APFs	200 V
L_f	Filter inductor	1.2 mH
L_g	Grid inductor	800 μH
L_d	Load inductor	1.2 mH
C_d	Load capacitor	100 μF
R_d	Load resistor	20 Ω/30 Ω
δ_1	APF1 droop coefficient (PB)	0.05/0.025/0.01
δ_2	APF2 droop coefficient (PB)	0.05
k	Harmonic parameter in CS method	20
δ_{CS1}	APF1 droop coefficient (CS)	1
δ_{CS2}	APF2 droop coefficient in (CS)	1/9
f	Switching frequency	20 kHz
T_d	Sampling time	50 μs(20 kHz)
	Modulating method	SVPWM

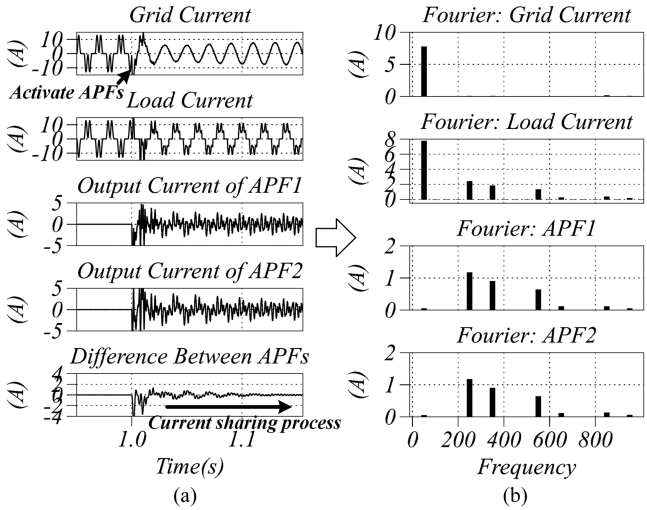

Fig. 24. Two APFs compensate for the harmonics in the ratio of 1:1. (a) Simulation waveforms. (b) Corresponding spectrum.

In Figs. 24–26, the waveforms and spectrums of current allocation are shown. In this process, the APFs charge the dc capacitors first and then start the harmonic compensation and current sharing. Therefore, the instant impact can be observed in these figures. But the charging impact will not influence the current sharing process, which is much slower.

In Fig. 24(a), the APFs are activated at $t = 1.0\,s$ and droop coefficients are assigned 0.05. According to the current difference result, the current sharing is achieved in 0.15 s. Fig. 24(b) verifies that APFs compensate for the harmonics successfully and achieve the capacity allocation in the ratio of 1:1. It can be aware that the fifth harmonic component in the load current is

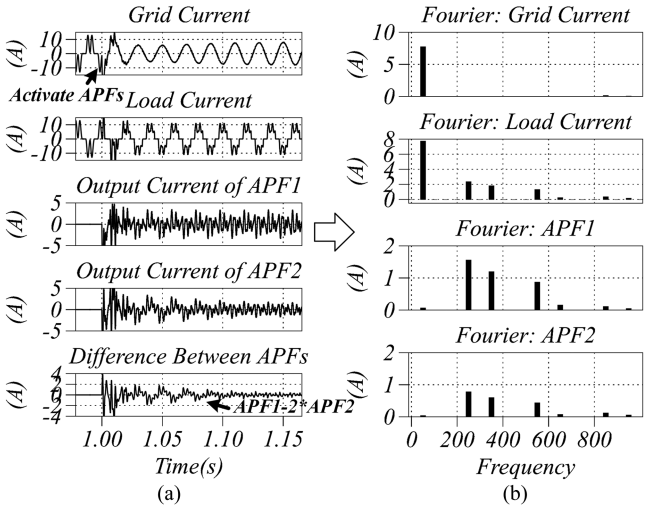

Fig. 25. Two APFs compensate for the harmonics in the ratio of 2:1. (a) Simulation waveforms. (b) Corresponding spectrum.

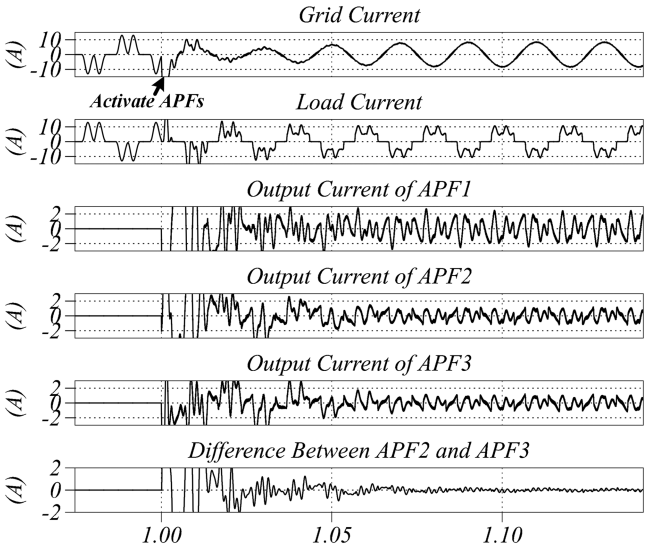

Fig. 26. Three APFs compensate for the harmonics in the ratio of 2:1:1.

2.39 A and each APF compensates 1.17 A, which is consistent with the theoretical analysis. Besides, this result remains the same for other designed specific harmonics (7th, 11th, 13th).

Similarly, Fig. 25 demonstrates the waveforms and spectrum of 2:1 current allocation. When APFs are activated at $t = 1.0\,s$, the harmonic compensation is achieved first. And then the current sharing is completed around $t = 1.15\,s$ with a relatively slower response. This phenomenon is consistent with the conclusion in Fig. 21, where the poles of current sharing are closer to the imaginary axis. As Fig. 25(b) depicts, the fifth harmonic component in the load current remains 2.39 A while APF1 compensates for 1.56 A and APF2 compensates for 0.78 A. Therefore, the feasibility of the proposed scheme and steady error analysis are verified in the case of two APFs.

Furthermore, to verify the effectiveness of the proposed scheme in more APFs, Fig. 26 depicts the current allocation

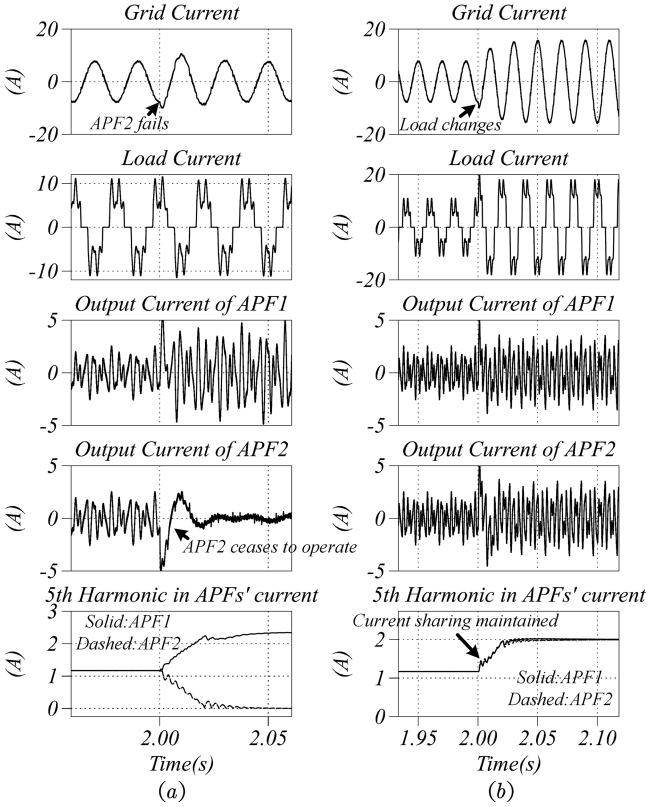

Fig. 27. Dynamic response of multiparalleled APFs in different situations. (a) One of the APFs ceases to operate. (b) Load is perturbated.

of three multiparalleled APFs. The coefficients are set as 0.025, 0.05,0.05 among APFs, and 2:1:1 current allocation is achieved. Besides, the dynamic response speed is basically the same as Fig. 24, verifying the analysis in Section III. Synthesizing Figs. 24–26, it is verified that the proposed droop control scheme can allocate the current of APFs in proportion.

Besides, to further verify the dynamic response analysis, Fig. 27 depicts the dynamic process of APFs in different situations. The amplitudes of the fifth harmonic in APFs' current are calculated to demonstrate the dynamic waveform. In Fig. 27(a), when APF2 ceases to operate at $t = 2\,s$, APF1 reacts rapidly to fulfill the vacancy in 0.05 s. And the distortion of grid current is eliminated in one period, demonstrating excellent response speed and redundancy control. Once one APF is broken accidentally, the other APFs could form a new droop relationship to maintain the filtering performance in time. Fig. 27(b) shows the case of load perturbation. When the load current increases at $t = 2\,s$, both APFs respond to the change and reach the new current sharing state in 0.05 s. As the fifth harmonic in APFs' current demonstrates, the current sharing is still maintained during the dynamic process. Fig. 27(a) and (b) both verify the excellent dynamic response and stability of the proposed scheme. Robust performance is obtained under varying working conditions.

Figs. 28 and 29 examine the differences between PB and CS methods, which are discussed in Section IV. Fig. 28 confirms the stability of the CS method in high filtering demand. When

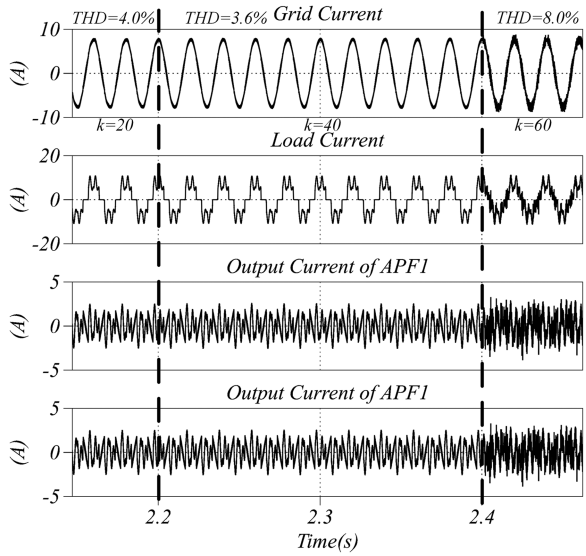

Fig. 28. Multiparalleled APFs' reaction to the increasing filtering demand in the CS method.

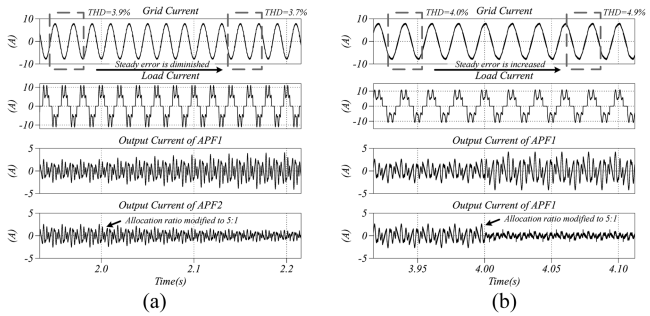

Fig. 29. Multiparalleled APFs' reaction to the changed allocation ratio. (a) PB method. (b) CS method.

parameter k increases from 20 to 60 to improve the filtering performance, the oscillation will be induced. It verifies that the filtering performance of the CS method is restricted by the system's stability. Fig. 29 illustrates the changes in the steady error of the PB method and CS method. As Fig. 29(a) shows, when the allocation ratio in the PB method is modified to 5:1, the THD of grid current decreases from 3.9% to 3.7% and dynamic speed slows down. But in the same case of the CS method as Fig. 29(b), the THD increases to 4.9%, destroying the filtering performance. This phenomenon verifies that the unbalanced allocation will increase the steady error in the CS method. And it further indicates the restriction between filtering performance and allocation range in the existing scheme. In comparison, the proposed scheme removes the constraint effectively. Its filtering error can be guaranteed under unbalanced allocation.

B. Prototype Experiments Under Various Operating Conditions

Experiments are conducted to verify the analysis, including prototype and hardware-in-the-loop (HIL) experiments. While

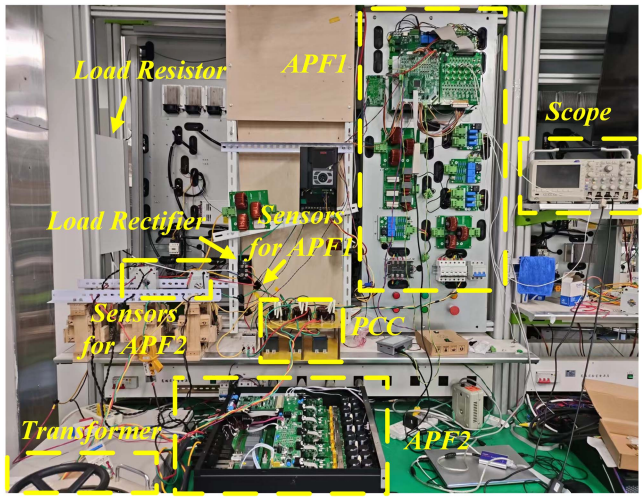

Fig. 30. Experiment platform.

prototype experiments are designed for the case of two multiparalleled APFs, HIL experiments are introduced mainly for more APFs. The prototype topology remains the same as the simulation. And the experiment platform is built as Fig. 30. To prove the feasibility of the proposed scheme, two different types of APF are selected as APF1 and APF2. Besides, two kinds of sensors are utilized to meet the requirements of APF1 and APF2. The experiments' control parameters remain the same as the simulations except that grid voltage is set around 40 V (Magnitude-phase) to simulate the industrial applications.

Fig. 31 depicts the waveforms of multiparalleled APFs without the proposed scheme. According to Fig. 31, APF1 and APF2 manage to achieve the harmonic compensation. However, the current oscillation occurs between APF1 and APF2. Compared with the simulations in Fig. 7, Fig. 31(a) shows the varying process of current sharing as measurement error exists. And the phase error can be observed according to Fig. 31(b). Without the proposed scheme, APFs lack the ability to stabilize the current sharing rapidly. It seriously deteriorates the system stability and reduces the compensation efficiency.

Figs. 32 and 33 depict the waveforms with the proposed scheme implemented. In Fig. 32(a), after APF1 is activated, the APF1's current is increasing rapidly and current sharing is completed without oscillations. Fig. 32(b) shows the zoomed steady waveforms in Fig. 32(a). It can be found that there is no phase error between APF1's current and APF2's current. And the 1:1 current allocation is achieved. Similar to Fig. 32, 1:2 current allocation is shown in Fig. 33 by changing the droop coefficient of APF1. It verifies the effectiveness and feasibility of the proposed scheme. Besides, the dynamic response speed and steady error remain consistent in Figs. 32 and 33. This phenomenon is identical to the simulations in Figs. 24 and 25, verifying the scheme's immunity to parameter variations.

Fig. 34 demonstrates the expandability and redundancy of the proposed scheme. In this case, the droop coefficient of APF1 is assigned 0 and APF2 is operated all the time. Therefore, when APF1 is activated in Fig. 34(a), it compensates for most

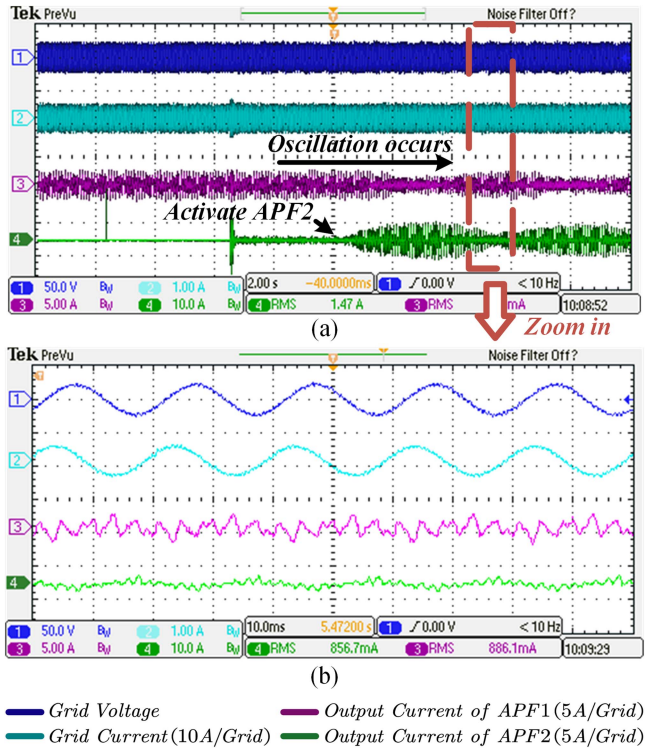

Fig. 31. Waveforms of multiparalleled APFs' reaction without proposed droop scheme implemented. (a) Oscillation occurs between APF1. (b) Zoomed region. (B-phase grid current).

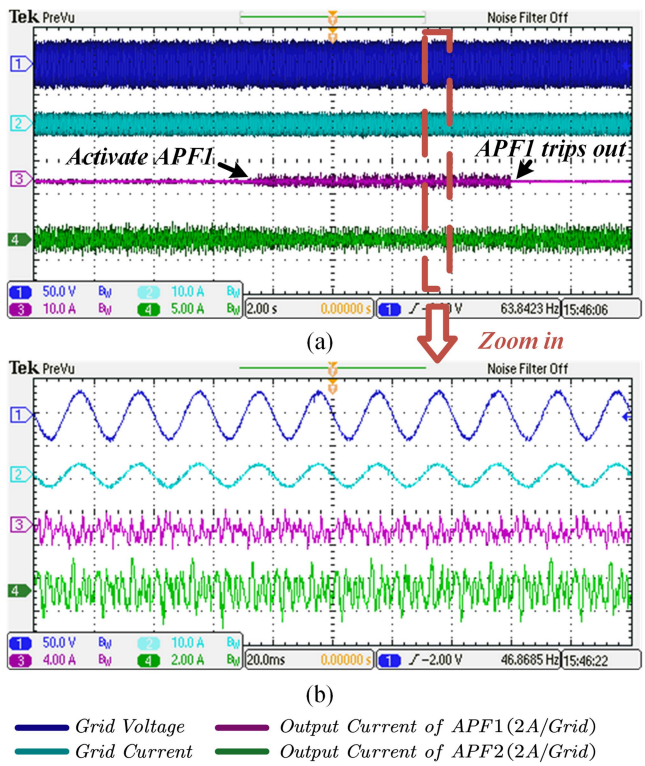

Fig. 32. Waveforms of multiparalleled APFs with the proposed scheme in the ratio of 1:1. (a) Waveform of current sharing. (b) Zoomed steady state.

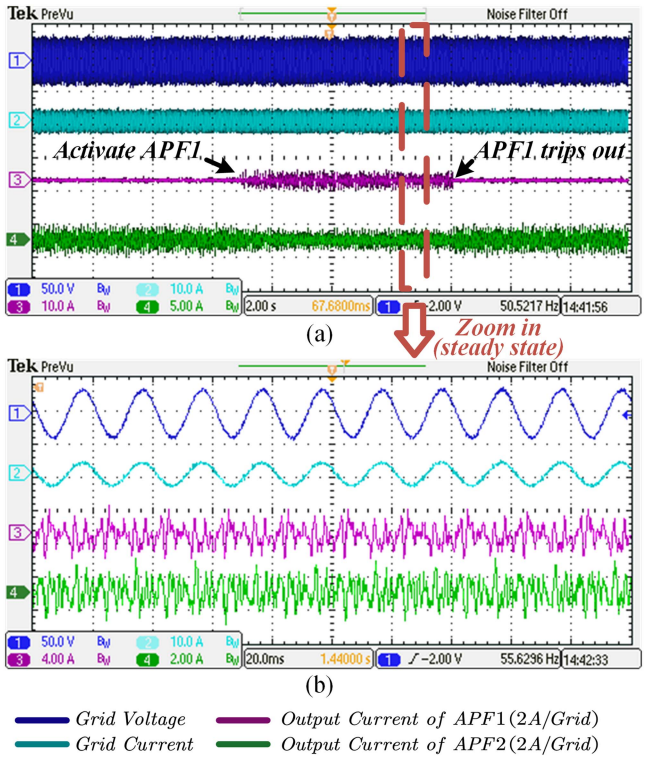

Fig. 33. Waveforms of multiparalleled APFs with the proposed scheme in the ratio of 1:2. (a) Waveform of current sharing. (b) Zoomed steady state.

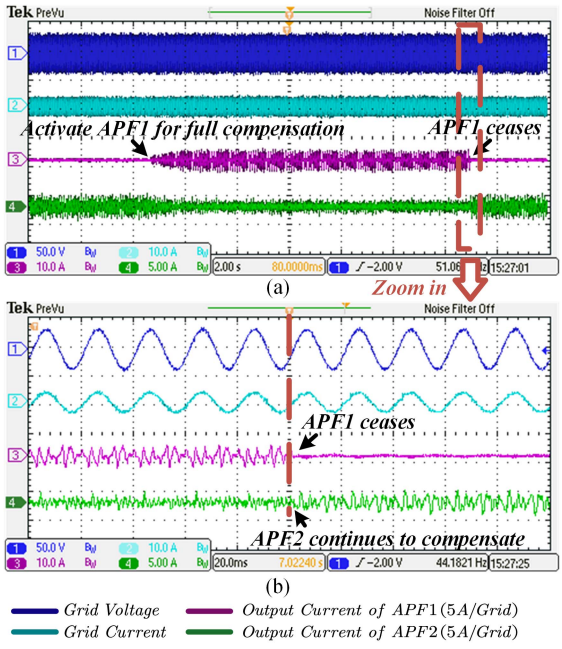

Fig. 34. Waveforms of multiparalleled APFs demonstrating the startup and halted state. (a) Waveform of the overall process. (b) Zoomed waveforms when APF1 trips out.

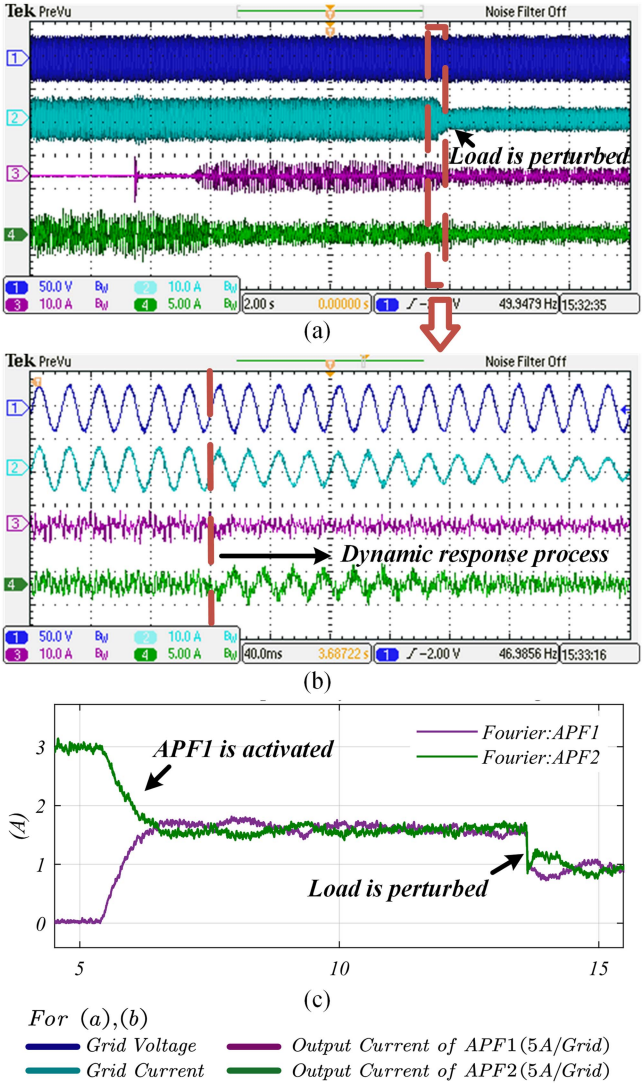

Fig. 35. Waveforms of multiparalleled APFs' dynamic response to load perturbation. (a) Waveform of the overall process. (b) Dynamic process when the load is perturbated. (c) Fifth harmonic amplitude of APFs' current in (a).

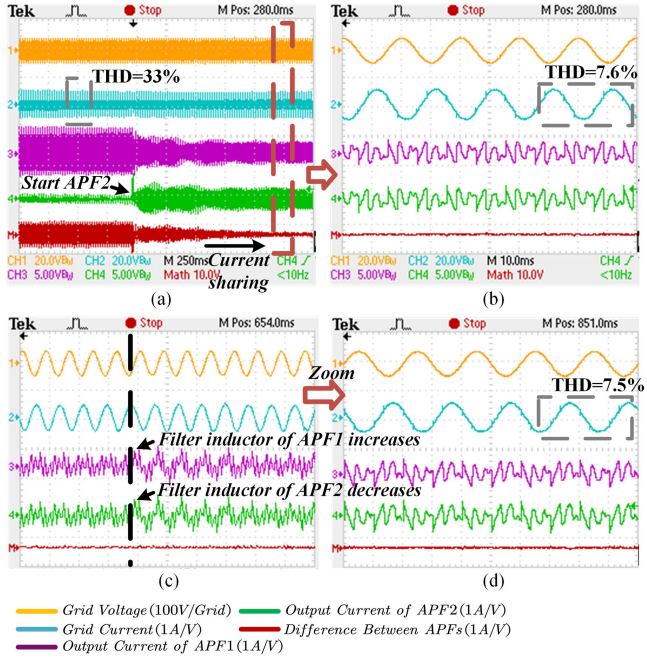

Fig. 36. Waveforms of two APFs operated in parallel (1:1). (a) Start-up process. (b) Steady state in (a). (c) Dynamic response of inductor variations. (d) Steady state in (b).

harmonics due to the droop relationship. And APF2 gives up the compensation. In this process, the allocation adjusting process has been performed. It illustrates that once an additional APF is installed, the droop relationship will allocate the current automatically. Therefore, the expandability of the proposed scheme is verified. Furthermore, when APF1 trips out in Fig. 34(b), APF2 reacts rapidly to compensate for the harmonics. It shows that when a specific APF fails, it can be directly disconnected and other APFs will automatically compensate the vacancy. The phenomenon is consistent with the simulations in Fig. 27(a). Therefore, the redundancy control is verified.

Furthermore, Fig. 35(a) and (b) show the dynamic response of multiparalleled APFs when the load is perturbed from 10 to 20 Ω. And Fig. 35(c) depicts the fifth harmonic amplitude of APFs' current in the whole dynamic process. In Fig. 35, when the load is perturbed at $t = 13.6\,s$, the current sharing of harmonics is completed rapidly. Different from the simulations in Fig. 27(b), the fundamental current reacts to the impact more slowly due to the current protection. Fig. 35(b) and (c) show that the current sharing has reached the proper current sharing state after the impact. It effectively verifies the analysis of system stability and dynamic response. Robust performance is achieved by the proposed scheme under varying loads. Besides, Fig. 35(c) also records the dynamic process of APF activation at $t = 5.4\,s$. It reveals that APF1 and APF2 form the droop relationship and share the compensation current successfully.

C. HIL Experiment Results

To verify the proposed scheme in more APFs, experiments are conducted in the HIL platform MT6020. MT6020 uses FPGA to simulate the hardware and supports algorithm verification in multiple inverters. In this section, the cases of 2, 3, and 4 APFs operated in parallel are considered. Dynamic response and parameter immunity of the proposed scheme are further examined.

Fig. 36 depicts the dynamic response of start-up and inductor variations in two multiparalleled APFs. In Fig. 36(a), the red line represents the difference between APFs' current. And it decreases to zero after APF2 is activated, which shows the current sharing process clearly. Fig. 36(b) shows the zoomed steady waveforms of Fig. 36(a). It is consistent with the current sharing results of simulations and prototype experiments. Fig. 36(c) and (d) illustrate dynamic/steady response of filter inductor variations. In this case, the filter inductor of APF1 is increased to 120% of its nominal value and that of APF2 decreases to 80% simultaneously. In this extreme condition, the current sharing is achieved and the impact is eliminated

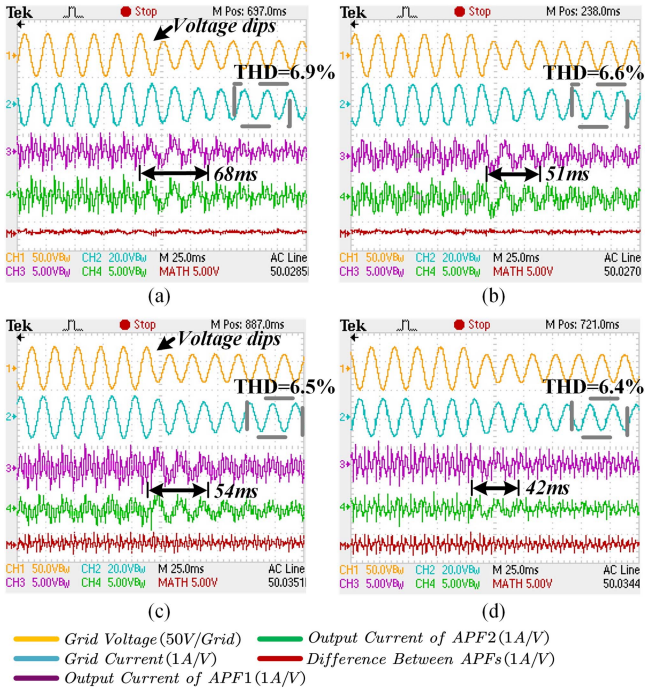

Fig. 37. Waveforms of two APFs operated under grid voltage sag. (a) 1:1 allocation with smaller controllers' gain. (b) 1:1 allocation with larger controllers' gain. (c) 2:1 allocation with smaller controllers' gain. (d) 2:1 allocation with larger controllers' gain.

in 0.125 s. In comparison with Fig. 36(b), grid current's THD remains basically constant at 7.5% despite the variation of inductors. It successfully verifies the immunity of the proposed scheme to the inductors' variations.

In Fig. 37, the performance of the proposed scheme is evaluated under grid voltage sag. And various sets of control parameters are assigned to verify the reliability. 1:1 current allocation is set in Fig. 37(a) and (b), while 2:1 is set in (c) and (d). The proposed scheme exhibits robust performance when grid voltage abruptly decreases to 30 V (RMS). The sudden impact is eliminated in 70 ms. And the THD of grid current decreases by up to 0.2%. Both the filtering performance and current allocation are not influenced by the voltage sag. Besides, the immunity of the proposed scheme is further verified in Fig. 37. The proportional gain of APF1's controller is specified as 3 in Fig. 37(a) and (c). The same parameter's value is 6 in (b) and (d). With larger controller's gain, the dynamic response speed is improved from 68 to 51 ms in Fig. 37(a) and (b). Similar improvement can also be found in (c) and (d) (54–41 ms). THD is slightly decreased from 6.9% to 6.6% in Fig. 37(a) and (b). The same THD variation can be observed in (c) and (d), which decreases from 6.5% to 6.4%. The modest variations verify that the filtering performance of the proposed scheme is unaffected. High-frequency harmonics are the main causes of THD variations, which is irrelevant to the proposed scheme.

The cases of three and four multiparalleled APFs are depicted in Figs. 38 and 39 with 10 Ω load resistor, respectively. In Fig. 38, the APFs realize the 1:1:1 reallocation successfully after APF3 is activated. And Fig. 38(b) shows that there is

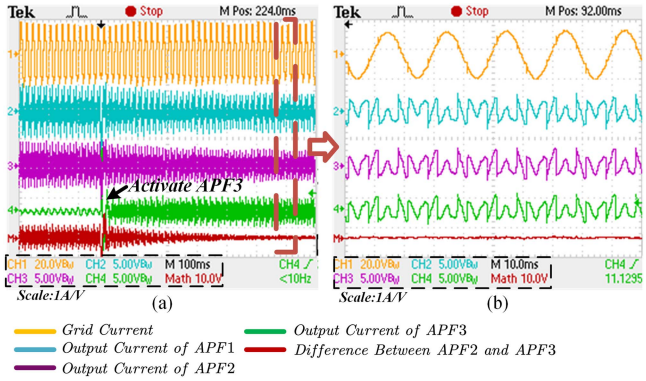

Fig. 38. Waveforms of three APFs operated in parallel (1:1:1). (a) Start-up process. (b) Steady state of current allocation.

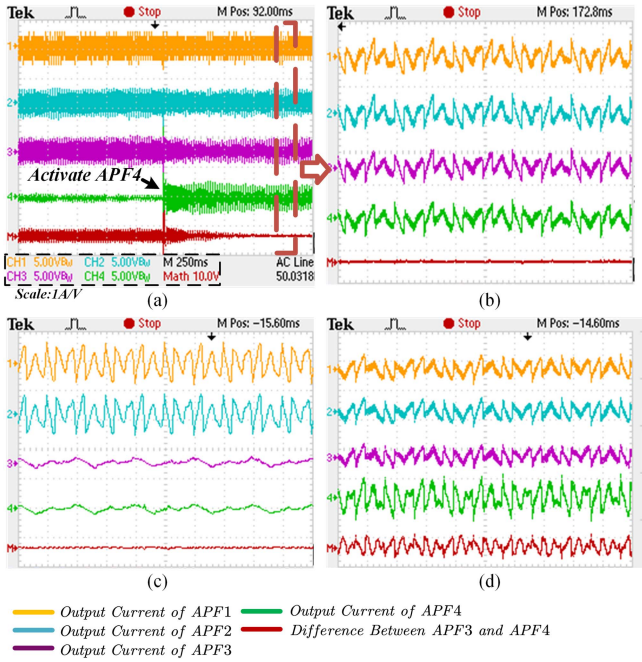

Fig. 39. Waveforms of four APFs operated in parallel. (a) Start-up process. (b) Current allocation in 1:1:1:1. (c) Current allocation in 1:1:0:0. (d) Current allocation in 1:1:1:2.

no phase error among APFs' current. Furthermore, four APFs are operated in parallel in Fig. 39. It realizes the equal current allocation among APFs in Fig. 39(a) and (b). As the red line shows, the performance of the proposed scheme does not deteriorate with the increasing APFs' number. Besides, different allocations of 1:1:0:0 and 1:1:1:2 are depicted in Fig. 39(c) and (d), respectively. It effectively verifies the flexibility of the proposed scheme. Compared with the simulations, additional high-frequency ripples can be observed with more APFs. By adjusting the modulation carriers as [18] and [19], minimum communication has the potential to address this problem. And performance of the proposed scheme will not be influenced.

VI. Conclusion

In this article, a novel decentralized droop control scheme for multiparalleled APFs with grid current detected was proposed.

Based on the power balance based control, the scheme enabled the APFs to allocate the compensation capacity in proportion to their rated capacity automatically. And it exhibited better filtering performance and allocation range.

First, the operating mechanism of the proposed droop control was illustrated with a case comprising two APFs. The droop relationship was realized by adding the feedback loop of each APF's output current with preset droop coefficients. Furthermore, the dynamic/steady performance analysis of the proposed scheme and corresponding parameter tuning algorithm were presented in this article. It was revealed that the proposed scheme could successfully achieve redundancy control and capacity allocation without communication. Additionally, excellent expandability, stability, and filtering performance were demonstrated. Robust performance was obtained under dynamic grid conditions. On this basis, the comparative analysis between the proposed scheme and the existing scheme was given in this article. The result demonstrated that the proposed scheme exhibited better filtering performance and allocation range. Additionally, the stability of the proposed scheme was also superior to that of the existing scheme which is restricted by filtering performance. Finally, extensive simulations and experiments were conducted, which effectively verified the viability of the proposed decentralized droop scheme.

On the basis of the proposed decentralized scheme, possible future research can be summarized as follows.

1) Incorporate minimum communication with the proposed scheme to further improve the filtering performance.
2) Analyze and suppress the resonance risk of the proposed scheme to enhance the scalability in larger systems.
3) The performance evaluation and stability analysis when multiparalleled APFs are integrated with other power quality improvement equipment (SVG, DVR …).

REFERENCES

[1] F. Briz, D. Díaz-Reigosa, M. W. Degner, P. García, and J. M. Guerrero, "Dynamic behavior of current controllers for selective harmonic compensation in three-phase active power filters," in *Proc. IEEE Energy Convers. Congr. Expo.*, 2011, pp. 2892–2899, doi: 10.1109/ECCE.2011.6064158.

[2] Z. Zhang, H. Yi, F. Zhuo, Y. Li, and X. Jiang, "Harmonic oscillation analysis and stabilization method comparison of shunt active power filter in full compensation mode," *IET Power Electron.*, vol. 17, no. 9, pp. 1145–1158, 2024, doi: 10.1049/pel2.12612.

[3] Y. Li, H. Yi, F. Zhuo, and X. Jiang, "Analysis and stabilization of APF systems considering dynamic of nonlinear loads," *IEEE Trans. Power Electron.*, vol. 39, no. 1, pp. 409–423, Jan. 2024, doi: 10.1109/TPEL.2023.3324650.

[4] D. Li, T. Wang, W. Pan, X. Ding, and J. Gong, "A comprehensive review of improving power quality using active power filters," *Electric Power Syst. Res.*, vol. 199, 2021, Art. no. 107389.

[5] A. Bhattacharya, C. Chakraborty, and S. Bhattacharya, "Parallel-connected shunt hybrid active power filters operating at different switching frequencies for improved performance," *IEEE Trans. Ind. Electron.*, vol. 59, no. 11, pp. 4007–4019, Nov. 2012, doi: 10.1109/TIE.2011.2173893.

[6] S. K. Khadem, M. Basu, and M. F. Conlon, "A review of parallel operation of active power filters in the distributed generation system," in *Proc. 14th Eur. Conf. Power Electron. Appl.*, 2011, pp. 1–10, doi: 10.1016/j.rser.2011.06.011.

[7] Q. Xu and G. Chen, "A novel control strategy for multi-modular shunt active power filter system," in *Proc. IEEE 11th Int. Conf. Power Electron. Drive Syst.*, 2015, pp. 1007–1012, doi: 10.1109/PEDS.2015.7203424.

[8] Y. Wang, Q. Xu, and G. Chen, "Simplified multi-modular shunt active power filter system and its modelling," *IET Power Electron.*, vol. 8, no. 6, pp. 967–976, 2015, doi: 10.1049/iet-pel.2014.0572.

[9] Z. Wu, G. Xu, W. Zhu, and G. Sheng, "The stability analysis and control strategies of multiparalleled SAPFs: A comprehensive overview," *IEEE Trans. Power Electron.*, vol. 39, no. 6, pp. 7444–7457, Jun. 2024, doi: 10.1109/TPEL.2023.3304379.

[10] Y. Xie, H. Yi, F. Zhuo, Y. Li, X. Jiang, and Z. Zhang, "Analysis and stabilization for full harmonic compensation oscillation in SAPF system with source current direct control," *IET Power Electron.*, vol. 17, no. 1, pp. 107–120, 2024, doi: 10.1049/pel2.126198.

[11] K. Liu et al., "Admittance modeling, analysis, and reshaping of harmonic control loop for multiparalleled SAPFs system," *IEEE Trans. Ind. Inform.*, vol. 17, no. 1, pp. 280–289, Jan. 2021, doi: 10.1109/TII.2020.2968374.

[12] L. L. D. Souza, N. Rocha, D. A. Fernandes, R. P. R. de Sousa, and C. B. Jacobina, "Grid harmonic current correction based on parallel three-phase shunt active power filter," *IEEE Trans. Power Electron.*, vol. 37, no. 2, pp. 1422–1434, Feb. 2022, doi: 10.1109/TPEL.2021.3107399.

[13] H. Yi et al., "A source-current-detected shunt active power filter control scheme based on vector resonant controller," *IEEE Trans. Ind. Appl.*, vol. 50, no. 3, pp. 1953–1965, May/Jun. 2014, doi: 10.1109/TIA.2013.2289956.

[14] S. J. Chiang and J. M. Chang, "Design and implementation of the parallelable active power filter," in *Proc. 30th Annu. IEEE Power Electron. Specialists Conf.*, 1999, vol. 1, pp. 406–411, doi: 10.1109/PESC.1999.789037.

[15] H.-S. Nien, T.-F. Wu, H.-M. Hsieh, and C.-L. Shen, "A parallel-APF system with current sharing controller and load-path control center to improve dynamic response and achieve weighting current distribution," in *Proc. 37th IEEE Power Electron. Specialists Conf.*, 2006, pp. 1–7, doi: 10.1109/pesc.2006.1712001.1.

[16] S. K. Khadem, M. Basu, and M. F. Conlon, "Parallel operation of inverters and active power filters in distributed generation system—A review," *Renewable Sustain. Energy Rev.*, vol. 15, no. 9, pp. 5155–5168, 2011, doi: 10.1016/j.rser.2011.06.011.

[17] S. Zhang, K. Dai, B. Xie, and Y. Kang, "Parallel control of shunt active power filters with capacity proportion frequency allocation," in *Proc. Int. Conf. Power Electron. Drive Syst.*, 2009, pp. 127–131, doi: 10.1109/PEDS.2009.5385854.

[18] Y. Wang, J. Gu, R. Chen, L. Qin, and J. Chen, "The multi-modular shunt APF based on direct current control and frequency doubling carrier phase-shifted SPWM," in *Proc. IEEE ECCE Asia Downunder*, 2013, pp. 867–871, doi: 10.1109/ECCE-Asia.2013.6579206.

[19] X. Bao, F. Zhuo, B. Liu, and Y. Tian, "Suppressing switching frequency circulating current in parallel inverters with carrier phase-shifted SPWM technique," in *Proc. IEEE Int. Symp. Ind. Electron.*, 2012, pp. 555–559, doi: 10.1109/ISIE.2012.6237147.

[20] K. Liu, W. Cao, and J. Zhao, "Dual-loop-based harmonic current control strategy and admittance modeling for a multimodular parallel SAPFs system," *IEEE Trans. Ind. Electron.*, vol. 67, no. 7, pp. 5456–5466, Jul. 2020, doi: 10.1109/TIE.2019.2934068.

[21] K. Liu, W. Cao, J. You, Y. Huang, J. Zhao, and J. Song, "Improved parallel operation for multi-modular shunt APF using dual harmonic compensation loop," in *Proc. IEEE 8th Int. Power Electron. Motion Control Conf.*, 2016, pp. 126–130, doi: 10.1109/IPEMC.2016.7512273.

[22] S. Leng, I.-Y. Chung, and D. A. Cartes, "Distributed operation of multiple shunt active power filters considering power quality improvement capacity," in *Proc. 2nd Int. Symp. Power Electron. Distrib. Gener. Syst.*, 2010, pp. 543–548, doi: 10.1109/PEDG.2010.5545917.

[23] A. H. Yazdavar, M. A. Azzouz, and E. F. El-Saadany, "A novel decentralized control scheme for enhanced nonlinear load sharing and power quality in islanded microgrids," *IEEE Trans. Smart Grid*, vol. 10, no. 1, pp. 29–39, Jan. 2019, doi: 10.1109/TSG.2017.2731217.

[24] X. Zhao, L. Meng, C. Xie, J. M. Guerrero, and X. Wu, "A unified voltage harmonic control strategy for coordinated compensation with VCM and CCM converters," *IEEE Trans. Power Electron.*, vol. 33, no. 8, pp. 7132–7147, Aug. 2018.

[25] P. Sreekumar and V. Khadkikar, "Direct control of the inverter impedance to achieve controllable harmonic sharing in the islanded microgrid," *IEEE Trans. Ind. Electron.*, vol. 64, no. 1, pp. 827–837, Jan. 2017, doi: 10.1109/TIE.2016.2574308.

[26] F. Deng, W. Yao, X. Zhang, Y. Tang, and P. Mattavelli, "Review of impedance-reshaping-based power sharing strategies in islanded AC microgrids," *IEEE Trans. Smart Grid*, vol. 14, no. 3, pp. 1692–1707, May 2023, doi: 10.1109/TSG.2022.3208752.

[27] G. Falahi and H. Mokhtari, "Performance improvement of parallel active power filters using droop control method," in *Proc. Asia-Pacific Power Energy Eng. Conf.*, 2009, pp. 1–4, doi: 10.1109/APPEEC.2009.4918590.
[28] T. G. Vaidya and K. Chatterjee, "A decentralized control scheme for multimodular shunt active harmonic filters," *IEEE Trans. Ind. Electron.*, vol. 69, no. 2, pp. 1081–1090, Feb. 2022, doi: 10.1109/TIE.2021.3053898.
[29] C. Gao, S. He, P. Davari, F. Blaabjerg, K. N. Leung, and P. C. Loh, "A decentralized control scheme for active power filter parallel system," in *Proc. 49th Annu. Conf. IEEE Ind. Electron. Soc.*, 2023, pp. 1–5, doi: 10.1109/IECON51785.2023.10311852.
[30] W.-K. Sou, C.-W. Chao, C. Gong, C.-S. Lam, and C.-K. Wong, "Analysis, design, and implementation of multi-quasi-proportional-resonant controller for thyristor-controlled LC-coupling hybrid active power filter (TCLC-HAPF)," *IEEE Trans. Ind. Electron.*, vol. 69, no. 1, pp. 29–40, Jan. 2022, doi: 10.1109/TIE.2021.3050393.
[31] J. Li, F. Zhuo, X. Wang, L. Wang, and S. Ni, "A grid-connected PV system with power quality improvement based on boost + dual-level four-leg inverter," in *Proc. IEEE 6th Int. Power Electron. Motion Control Conf.*, 2009, pp. 436–440, doi: 10.1109/IPEMC.2009.5157427.
[32] S. Busoand and P. Mattavelli, *Digital Control in Power Electronics*. San Rafael, CA, USA: Morgan & Claypool, 2015.

Zhilong Zhang (Student Member, IEEE) was born in Hubei, China, in 2000. He received the B.S. degree in electrical engineering in 2022 from Xi'an Jiaotong University, Xi'an, China, where he is currently working toward the Ph.D. degree in electrical engineering with the Department of Electrical Engineering.

His research interests include modeling and analysis of dc/ac converters.

Hao Yi (Member, IEEE) received the Ph.D. degree in electrical engineering from Xi'an Jiaotong University (XJTU), Xi'an, China, in 2013.

From 2016 to 2017, he was with the Department of Energy Technology, Aalborg University, Aalborg, Denmark. He is currently a Professor with XJTU. He hosted 1 prize and has authored or coauthored more than 70 articles on the topics of his research interests, which include power electronics technologies used in power quality control, distributed power control, and grid-connected converter modeling/control.

Yuguo Li (Student Member, IEEE) was born in Sichuan, China, in 1996. He received the B.S. degree in electrical engineering in 2018 from Xi'an Jiaotong University, Xi'an, China, where he is currently working toward the Ph.D. degree with the Department of Electrical Engineering.

His research interests include power quality and control of power electronic converters.

Xin Jiang (Student Member, IEEE) was born in Sichuan, China, in 1998. He received the B.S. degree in electrical engineering from Sichuan University, Chengdu, China, in 2020. He is currently working toward the Ph.D. degree in electrical engineering with the Department of Electrical Engineering, Xi'an Jiaotong University, Xi'an, China.

His research interests include small signal stability and control of power electronic converters.

Zhenxiong Wang (Member, IEEE) received the B.S. and Ph.D. degrees in electrical engineering from Xi'an Jiaotong University, Xi'an, China, in 2014 and 2021, respectively.

He is currently an Assistant Professor with Xi'an Jiaotong University. His research interests include grid-forming control strategy and microgrid.

Fang Zhuo (Member, IEEE) was born in Shanghai, China, in 1962. He received the B.S. degree in automatic control and the M.S. and Ph.D. degrees in automation and electrical engineering from Xi'an Jiaotong University (XJTU), Xi'an, China, in 1984, 1989, and 2001, respectively.

In 1996, he was an Associate Professor with XJTU, where he became a Full Professor of power electronics and drives in 2004. He was a supervisor of Ph.D. students. He is the key finisher of the four projects sponsored by the National Natural Science Foundation of China and more than 40 projects cooperated with companies from the industry. He holds four patents. His research interests include power electronics, power quality, active power filter, reactive power compensation, and inverters for distributed power generation.

Dr. Zhuo is a Member of the China Electro Technical Society, the Automation Society, and the Power Supply Society. He received four provincial- and ministerial-level science and technology advancement awards. He is also the Power Quality Professional Chairman of the Power Supply Society in China.